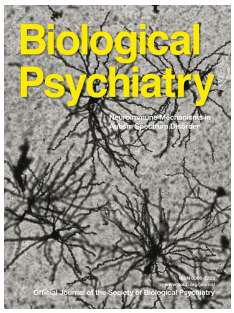
Journal Pre-proof



Excitation-Inhibition Balance and Fronto-Limbic Connectivity Distinguish TMS Treatment Outcomes in Refractory Depression

Davide Momi, Zheng Wang, Mohammad P. Oveisi, Kevin Kadak, Sorenza P. Bastiaens, Jennifer I. Lissemore, Yoshihiro Noda, Jonathan Downar, Fidel Vila Rodriguez, Rebecca Strafella, Zafiris J. Daskalakis, Christoph Zrenner, Reza Zomorrodi, Camarin E. Rolle, Manish Saggar, Nolan Williams, Corey J. Keller, Daniel M. Blumberger, Daphne Voineskos, John D. Griffiths

PII: S0006-3223(26)01591-X

DOI: https://doi.org/10.1016/j.biopsych.2026.09.027

Reference: BPS 16247

To appear in: *Biological Psychiatry*

Received Date: 29 April 2026

Revised Date: 29 September 2026

Accepted Date: 29 September 2026

Please cite this article as: Momi D., Wang Z., Oveisi M.P., Kadak K., Bastiaens S.P., Lissemore J.I., Noda Y., Downar J., Rodriguez F.V., Strafella R., Daskalakis Z.J, Zrenner C., Zomorrodi R., Rolle C.E., Saggar M., Williams N., Keller C.J., Blumberger D.M., Voineskos D. & Griffiths J.D., Excitation-Inhibition Balance and Fronto-Limbic Connectivity Distinguish TMS Treatment Outcomes in Refractory Depression, *Biological Psychiatry* (2026), doi: https://doi.org/10.1016/j.biopsych.2026.09.027.

This is a PDF of an article that has undergone enhancements after acceptance, such as the addition of a cover page and metadata, and formatting for readability. This version will undergo additional copyediting, typesetting and review before it is published in its final form. As such, this version is no longer the Accepted Manuscript, but it is not yet the definitive Version of Record; we are providing this early version to give early visibility of the article. Please note that Elsevier's sharing policy for the Published Journal Article applies to this version, see: https://www.elsevier.com/about/policies-and-standards/sharing#4-published-journal-article. Please also note that, during the production process, errors may be discovered which could affect the content, and all legal disclaimers that apply to the journal pertain.

© 2026 Published by Elsevier Inc on behalf of Society of Biological Psychiatry.

Journal Pre-proof

Excitation-Inhibition Balance and Fronto-Limbic Connectivity Distinguish TMS Treatment Outcomes in Refractory Depression

Davide Momi[1,2,3,4], Zheng Wang[1], Mohammad P. Oveisi[1,5], Kevin Kadak[1,6], Sorenza P. Bastiaens[1,6], Jennifer I. Lissemore[2], Yoshihiro Noda[7,8], Jonathan Downar[9], Fidel Vila Rodriguez[10,11], Rebecca Strafella[12], Zafiris J Daskalakis[13], Christoph Zrenner[12], Reza Zomorrodi[12], Camarin E. Rolle[2], Manish Saggar[2], Nolan Williams[2], Corey J. Keller[2,3,14], Daniel M. Blumberger[12], Daphne Voineskos[12], John D. Griffiths[1,5,6,8]

1 Krembil Centre for Neuroinformatics, Centre for Addiction and Mental Health (CAMH), Toronto, Canada.
2 Department of Psychiatry and Behavioral Sciences, Stanford University Medical Center, Stanford, CA, USA.
3 Wu Tsai Neurosciences Institute, Stanford University, Stanford, CA, USA.
4 Noel Drury, M.D. Institute for Translational Depression Discoveries, University of California, Irvine, CA, USA
5 Institute of Biomedical Engineering, University of Toronto, Toronto, Canada.
6 Institute of Medical Science, University of Toronto, Toronto, Canada.
7 Department of Neuropsychiatry, Keio University School of Medicine, Tokyo, Japan
8 Department of Psychiatry, Mita Hospital, International University of Health and Welfare, Tokyo, Japan
9 Department of Psychiatry, Temerty Faculty of Medicine, University of Toronto, Toronto, Ontario, Canada.
10 Non-Invasive Neurostimulation Therapies Laboratory, Department of Psychiatry, Faculty of Medicine, University of British Columbia, Vancouver, BC, Canada
11 School of Biomedical Engineering, Faculty of Applied Science | Faculty of Medicine, University of British Columbia, Vancouver, BC, Canada
12 Temerty Centre for Therapeutic Brain Intervention, Campbell Family Mental Health Research Institute, Centre for Addiction and Mental Health, Toronto, Ontario, Canada.
13 Department of Psychiatry, University of California San Diego, La Jolla, California.
14 Veterans Affairs Palo Alto Healthcare System, Palo Alto, CA, USA.

† Corresponding author: momi.davide89@gmail.com

Short title: Whole-brain models distinguish TMS outcomes in TRD

Journal Pre-proof

Journal Pre-proof

ABSTRACT

Background: Intermittent theta burst stimulation (iTBS) targeting the left dorsolateral prefrontal cortex (DLPFC) is effective for treatment-resistant depression, but outcomes remain variable. The neurophysiological mechanisms underlying response remain poorly understood, limiting precision neuromodulation.

Methods: We combined transcranial magnetic stimulation with electroencephalography (TMS-EEG) and connectome-based Jansen-Rit neural mass modeling to investigate the mechanistic basis of treatment efficacy in 90 patients with treatment-resistant depression. Individualized whole-brain models were fitted to pre- and post-iTBS TMS-evoked potentials, yielding subject-specific estimates of synaptic connectivity, excitation-inhibition (E/I) balance, and cortical dynamics. Brain states were defined by singular value decomposition of the model's population activity, and partial least squares analysis with nested cross-validation identified the brain-state pattern distinguishing responders from non-responders.

Results: We identified two neurophysiological signatures associated with treatment response. First, responders showed greater post-treatment reductions in 3–10 Hz oscillatory power, driven by shifts in E/I balance toward greater inhibitory control through reduced excitatory drive and increased inhibitory-to-pyramidal connectivity. Second, a pre-treatment brain state characterized by opposite-polarity dynamics between subgenual anterior cingulate cortex (sgACC) and left DLPFC distinguished responders from non-responders, consistent with prior fMRI findings on frontolimbic anticorrelation. Neural trajectory analysis further revealed greater dynamical reorganization and increased attractor stability in responders following treatment.

Conclusions: These findings provide a neurophysiologically-informed framework linking iTBS treatment efficacy to specific changes in cortical E/I balance and frontolimbic circuit dynamics, pointing toward candidate markers that, with subject-specific structural connectivity and independent validation, may inform personalized neuromodulation approaches in treatment-resistant depression.

Journal Pre-proof

INTRODUCTION

Major depressive disorder (MDD) affects over 350 million people worldwide and is a leading contributor to global disability (1). Only about 30% of patients achieve remission with first-line therapies, and a substantial fraction develop treatment-resistant depression (TRD) (2). Repetitive transcranial magnetic stimulation (rTMS), including FDA-approved intermittent theta burst stimulation (iTBS) of the left dorsolateral prefrontal cortex (DLPFC), is effective for TRD (3–6). However, response rates range from 29% to 46% (7,8), and treatment selection remains largely trial-and-error because the circuit-level changes distinguishing responders remain unclear.

Two lines of evidence point toward candidate mechanisms: cortical excitation-inhibition (E/I) balance and frontolimbic circuit dynamics.

TMS-EEG can index cortical excitability and inhibition through both stimulation-evoked responses and stimulation-induced oscillatory activity (9,10), and specific components of the TMS-evoked potential (TEP) serve as indirect markers of E/I state, which appears disrupted in MDD (11). Voineskos et al. (12) reported significant deficits in GABA-mediated cortical inhibition in patients with MDD relative to controls, consistent with broader evidence of altered GABA and glutamate across multiple brain regions in depression (13–15), and better clinical outcomes have been associated with pre-treatment markers such as a more negative N45 waveform and a smaller P60 amplitude (16), potentially reflecting enhanced GABAergic inhibition and reduced glutamatergic excitation, respectively.

The second lead concerns frontolimbic circuit dynamics: fMRI studies consistently show that stronger negative functional connectivity between the DLPFC stimulation site and subgenual anterior cingulate cortex (sgACC) at baseline predicts better treatment outcomes (17–20), suggesting that rTMS may act by modulating communication between these regions. Both leads remain inferential: TMS-EEG components and fMRI connectivity reflect scalp signals or slow hemodynamic fluctuations and do not directly identify the synaptic or effective-connectivity changes generating them; both also face signal-to-noise and spatial-resolution limitations (21,22). This measurement-to-circuit gap limits mechanistic understanding and prediction.

Whole-brain modeling (WBM) addresses this measurement-to-circuit gap by fitting a biophysically grounded generative model to each participant's TEPs and estimating the physiological parameters that generate the observed response (23,24). This provides two complementary capabilities. First, E/I balance is represented explicitly as the ratio of excitatory and inhibitory loop gains, allowing low-frequency power changes to be related to specific changes in modeled circuit physiology rather than left as spectral correlates. Second, anatomical connectivity constrains the estimation of DLPFC–sgACC dynamics, including for regions not directly observable at the scalp, allowing the fMRI-derived frontolimbic finding to be examined in an electrophysiologically informed framework. WBM has provided mechanistic insight across

neuropsychiatric and neurological conditions (25–29), but has not previously been used to link iTBS response in TRD to underlying circuit dynamics.

In this study, we combined longitudinal TMS-EEG with WBM in 90 patients with TRD to identify circuit features associated with iTBS response. Responders showed greater reductions in 3–10 Hz power accompanied by a modeled shift toward inhibitory control through reduced excitatory drive. We also identified a pretreatment pattern characterized by opposite-polarity DLPFC–sgACC dynamics that was associated with clinical outcome, an exploratory finding consistent with prior fMRI studies (17–19). Together, these findings link treatment response to spectral, physiological, and frontolimbic dynamics.

Journal Pre-proof

METHODS AND MATERIALS

The analyses comprised EEG preprocessing and calculation of TMS-evoked responses, construction of a diffusion MRI-derived anatomical connectivity prior, simulation and individual fitting of a connectome-based neural mass model, and statistical analysis of empirical and model-derived measures (Fig. 1).

Fig. 1. Overview of study design and methodological workflow for subject-specific connectome-based whole-brain modeling of TMS-evoked potentials. (A) Single-pulse TMS-EEG evoked responses and HRSD-17 depression scale were recorded before and after rTMS iTBS therapy consisting of 30 treatment sessions delivered over 6 weeks (5 days/week). Each daily treatment consisted of two 600-pulse iTBS sessions applied over the left DLPFC (1200 pulses total per day), delivered at 120% resting motor threshold as triplet 50 Hz bursts repeated at 5 Hz. Participants were randomized to a separated schedule (two sessions 54 minutes apart) or a contiguous schedule (two sessions 0 minutes apart), with sham sessions included to maintain blinding within each schedule; total daily dose was identical across schedules. For further details on the data collection and EEG preprocessing methodology see Strafella et al. (2023)(30). **(B)** Diffusion-weighted MRI tractography was computed from a sample of healthy young individuals from the HCP Dataset (31), and then averaged to give a grand-mean anatomical connectome. **(C)** The Jansen-Rit model (32) was embedded in each of the 200 nodes of the Schaefer atlas (33) for simulating and fitting neural activity time series. The TMS-induced depolarization of the resting membrane potential was modeled by a perturbing voltage offset to the mean membrane potential of the pyramidal cell. **(D)** A lead field matrix was then used for moving the parcels' time series into channel space and generating simulated TMS-EEG. **(E)** The goodness-of-fit (loss) was calculated between simulated and empirical TMS-EEG time series. Utilizing the autodiff-computed gradient (34) between the objective function and model parameters, model parameters were optimized using the ADAM algorithm (35). **(F)** Finally, the optimized model parameters were used to generate the fitted, simulated TMS-EEG activity, for which we report comparisons with the empirical data at both the channel and source level using conventional statistical techniques.

Recruitment and trial design

This analysis included 90 participants with treatment-resistant depression from a triple-blind randomized controlled trial conducted at the Centre for Addiction and Mental Health, University Health Network, and the University of British Columbia (ClinicalTrials.gov: NCT02729792) (36). Eligible participants were aged 18–59 years, met diagnostic criteria for MDD, had a baseline HRSD-17 score ≥18, and had failed at least one adequate antidepressant trial or been unable to tolerate two trials. Response was defined a priori as a ≥50% reduction in HRSD-17 from baseline to treatment end. Participants completed 30 treatment days over six weeks and received 1,200 active pulses per day to the left DLPFC at 120% resting motor threshold, delivered either as two 600-pulse iTBS sessions separated by 54 minutes or as one 1,200-pulse iTBS session paired with a sham session to maintain blinding and equalize treatment contact. The schedules were pooled because the total daily active dose was identical. Single-pulse TMS-EEG was acquired before the first and after the final treatment and therefore indexed cortical responsivity across the treatment course rather than the acute effects of iTBS. The study was approved in accordance with the Declaration of Helsinki, and all participants provided written informed consent. Complete eligibility, treatment, and acquisition details are provided in the Supplementary Methods and parent trial report (30).

144

145 **Overview of computational modelling approach**

146 The model comprised 200 cortical regions from the Schaefer seven-network atlas (33), coupled through a
147 population-representative structural connectome constructed from diffusion MRI data from 400 Human
148 Connectome Project participants (31). Each region contained a Jansen–Rit neural mass model (32)
149 representing pyramidal cells and excitatory and inhibitory interneurons, whose interactions generated
150 damped oscillatory responses that propagated through the connectome. TMS was modeled as an external
151 input, and simulated cortical activity was projected into EEG channel space using a lead-field matrix. The
152 model was fitted separately to each participant's pre- and post-iTBS TMS-EEG data, yielding session-
153 specific physiological and connectivity estimates conditioned on the shared normative connectome. Local
154 time constants and within-region connectivity parameters were participant-specific but spatially
155 homogeneous across the 200 regions; regional variation arose from the connectome and spatial distribution
156 of TMS input. Complete connectome, model, prior, and optimization procedures are provided in the
157 Supplementary Methods and previous reports (37,38); parameter priors and fitted distributions are shown
158 in Supplementary Table S1 and Fig. S1.

159

160 **Model goodness-of-fit**

161 Goodness-of-fit was assessed by comparing empirical and model-generated TMS-EEG waveforms against
162 1,000 time-wise permutations. Complete procedures and subject-level results are provided in
163 Supplementary Methods Section 1.5, Supplementary Results Section 2.3, and Fig. S3.

164

165 **Stimulus-induced spectral power analyses**

166 Stimulus-induced power from 2–50 Hz was calculated using Morlet wavelets, log-transformed, averaged
167 across trials, and evaluated from 0–300 ms relative to a −300–0 ms baseline. Within-participant post-versus-
168 pre changes were assessed using 1,000 permutations with cluster correction; responder versus non-
169 responder differences were evaluated using a second-level cluster-based permutation test with 1,000
170 iterations. Mean power change within the significant group-level cluster was extracted and related to
171 changes in fitted physiological parameters. Complete procedures and spectral maps are provided in
172 Supplementary Methods Section 1.6, Supplementary Results Sections 2.1 and 2.4, and Figs. S2 and S4.

173

174 **Physiological parameters and E/I balance**

175

176 We examined the excitatory and inhibitory time constants and four within-region connectivity parameters:
177 pyramidal-to-excitatory (P→E), excitatory-to-pyramidal (E→P), pyramidal-to-inhibitory (P→I), and

Journal Pre-proof

inhibitory-to-pyramidal (I→P) connectivity, representing the model's excitatory and inhibitory feedback pathways. A composite E/I ratio was calculated as [P→E × E→P]/[P→I × I→P] after mean-normalizing each parameter across participants and sessions; lower values indicated greater inhibitory relative to excitatory loop gain. Each parameter and the E/I ratio were analyzed using a 2 × 2 repeated-measures ANOVA with time as the within-participant factor and group as the between-participant factor. The threshold was Bonferroni-adjusted to $p<0.007$ across seven measures. Complete procedures are provided in Supplementary Methods Section 1.7.

Model-derived brain states

TMS-evoked model activity from −100–300 ms was extracted for all three neural populations across 200 regions and concatenated before singular value decomposition. The first 20 components, explaining 96% of the variance, were retained, and mean-centered PLS analysis (39,40) identified pretreatment brain-state expression associated with responder status. SVD and PLS were performed within 100 repeated 75% training/25% test splits; models were fitted only to training participants, and held-out participants were projected onto the training-derived components. Significance and regional reliability were evaluated using 5,000 permutations and 5,000 bootstrap samples, respectively. The sgACC was identified as the consistently highest-loading region across training folds rather than through inspection of the full sample. DLPFC–sgACC loadings, sgACC time courses, and discrimination using stratified 10-fold and leave-one-out cross-validation with permutation testing were then evaluated. Complete procedures are provided in Supplementary Methods Sections 1.8 and 1.9.

Neural trajectory analysis in model-derived state space

Three-dimensional trajectories were reconstructed from pyramidal, excitatory-interneuron, and inhibitory-interneuron activity (Fig. 5A). Treatment-related deviation was quantified as the point-wise distance between post- and pre-iTBS trajectories, whereas attractor stability was quantified as the distance between each post-iTBS trajectory and its stable fixed point. Fixed points were identified numerically and confirmed using the Jacobian matrix. Distance curves were summarized by area under the curve and compared between groups using separate two-sample permutation tests with 10,000 iterations. Complete procedures are provided in Supplementary Methods Section 1.10.

Full analysis and model-fitting code is available at https://github.com/Davi1990/Momi_et_al_2025 and https://github.com/griffithslab/whobpyt.

Journal Pre-proof

RESULTS

Higher inhibition in responders following iTBS

We first compared post-minus-pre iTBS time-frequency activity between responders and non-responders. Both groups showed reduced induced power after treatment, but responders had a significantly greater reduction at 3–10 Hz (Fig. 2A; 1,000 permutations, all clusters $p<0.05$, corrected), most pronounced approximately 50–200 ms after stimulation. Transient group differences at 30–50 Hz did not survive cluster-based permutation testing. Because the significant effect was a post-minus-pre difference, it represents a treatment-related correlate of response rather than a pretreatment predictor.

To relate this effect to circuit physiology, we examined parameters estimated from the individualized Jansen–Rit models. Each region contained interacting pyramidal-cell, excitatory-interneuron, and inhibitory-interneuron populations. Within the model, reduced pyramidal-to-excitatory connectivity (P→E) decreases recurrent excitatory drive, whereas increased inhibitory-to-pyramidal connectivity (I→P) strengthens inhibitory feedback. Both shift population-level E/I balance toward inhibition, although they represent effective connectivity rather than direct synaptic measurements. To reproduce the experimental perturbation, TMS was simulated by applying the modeled stimulation input to the left DLPFC according to the spatial distribution of the TMS-induced electric field.

In responders, post-minus-pre changes in P→E connectivity were positively correlated with changes in power within the significant 3–10 Hz band (Fig. 2B; $r=0.56$, $p<0.001$), whereas no association was observed in non-responders ($r=-0.06$, $p=0.61$). The correlations differed significantly between groups (Fisher's $Z=3.064$, uncorrected $p=0.0022$; Bonferroni-adjusted $p=0.0131$). Thus, the greater low-frequency power reduction observed in responders was associated with a greater reduction in excitatory feedback. The remaining physiological parameters showed no significant correlations with spectral modulation; complete results are reported in Supplementary Results Section 2.1 and Fig. S2.

To test whether reduced P→E connectivity could reproduce these effects, we reduced P→E by 10%, 30%, or 50% while holding the remaining fitted parameters constant. In the participant with the highest baseline HRSD-17 score (41), progressive reductions attenuated the TMS-evoked response, particularly its late components (Fig. 2C). At the group level, a 50% reduction produced a low-frequency power decrease resembling the empirical responder effect (Fig. 2D). Responders also showed reduced late empirical GMFA after iTBS, consistent with our previous analysis (30), and progressive P→E reductions similarly decreased simulated GMFA (Fig. 2E) (42). These simulations reproduce the direction of the empirical changes and support their dynamical plausibility but are not independent evidence of a treatment- or responder-specific effect. Complete procedures are provided in Supplementary Methods Section 1.11.

Fig. 2. iTBS therapy suppresses TEP low-frequency oscillatory power by modulating the level of inhibition. (A) Difference in iTBS-induced power changes (post-iTBS minus pre-iTBS) between responders and non-responders, showing significantly greater power reduction in the 3–10 Hz range in responders relative to non-responders. **(B)** Correlations between post-iTBS vs pre-iTBS changes in the P→E synaptic weights and power changes within the significant 3–10 Hz time-frequency region identified in Panel A. Responders show a significant positive correlation ($r = 0.56$, $p < 0.001$) while non-responders show no significant relationship ($r = -0.06$, $p = 0.61$). **(C)** Simulated effects of shifting E/I balance toward inhibition (via decreased P→E connectivity) for the participant with the highest Hamilton Depression Rating Scale score (indicating more severe MDD). This simulation reveals a notable reduction in TEP amplitude, especially in the late components, with increasing inhibition. **(D)** Group-level induced time-frequency spectral comparison between the original (0% increased inhibition) and a 50% inhibition-increased simulation, demonstrating a similar low-frequency reduction as observed in empirical data in Panel A. **(E)** GMFA for empirical data, with pre (dashed) vs. post (solid) responses shown for responders (top). GMFA across simulations with incremental inhibition (bottom) reveals a similar trend where increased inhibition is associated with a decrease in the late component amplitude for responders.

Responder-specific elevated inhibition after iTBS treatment

We next examined treatment-related changes across all fitted Jansen–Rit physiological parameters, independently of the significant 3–10 Hz spectral effect. Among the individual parameters, inhibitory-to-pyramidal connectivity (I→P; (c4)) showed a significant time × group interaction ($F(1,86)=29.11$, $p<0.001$) and a significant main effect of group ($F(1,86)=76.86$, $p<0.001$). Post hoc comparisons showed no difference between responders and non-responders before treatment ($t=-1.21$, $p=0.23$) but a significant post-iTBS difference ($t=-2.598$, $p=0.0147$), with responders exhibiting greater I→P connectivity (Fig. 3A). The remaining individual physiological parameters showed no significant time × group interactions and are reported in Supplementary Results Section 2.2.

Because I→P was the only individual parameter showing significant group effects, we examined its relationship with clinical outcome. Pretreatment I→P connectivity was negatively correlated with post-treatment HRSD-17 scores in responders (Fig. 3B; $r=-0.56$, $p<0.0001$), indicating that responders with greater pretreatment inhibitory feedback had lower depression severity after treatment. No association was observed in non-responders ($r=-0.04$, $p=0.71$). However, because this relationship was identified within the responder group, it characterizes a mechanism associated with response rather than providing an independent method for classifying patients before treatment.

The composite E/I ratio also showed a significant time × group interaction ($F(1,86)=38.29$, $p<0.001$) and a significant main effect of group ($F(1,86)=59.21$, $p<0.001$), surviving the Bonferroni-adjusted threshold of $p<0.007$. The groups did not differ before treatment ($t=0.82$, $p=0.19$) but differed significantly after iTBS ($t=10.088$, $p<0.001$). Responders showed a post-treatment reduction in the E/I ratio, indicating greater inhibitory relative to excitatory loop gain, whereas non-responders showed no comparable shift (Fig. 3C).

Together, the I→P and E/I results indicate that successful treatment was associated with enhanced inhibitory influence through both individual feedback parameters and their composite balance.

Fig. 3. iTBS therapy modifies inhibitory feedback in cortical circuits differently in responders and non-responders. (A) Strength of the inhibitory feedback loop for responders (green) and non-responders (yellow) post-iTBS therapy, as given by per-group distributions of estimated Inhibitory interneuron (I) to Pyramidal cell (P) population synaptic weights (I→P). Vertical dashed lines mark the pre-iTBS group means (green, responders; orange/yellow, non-responders); the groups did not differ at baseline ($t = -1.21$, $p = 0.23$). Filled curves show the post-iTBS distributions. Post-iTBS therapy, responders exhibit an increase in inhibitory feedback, while non-responders show the opposite effect. **(B)** Pre-iTBS I→P synaptic weights show differential correlations with post-treatment depression severity (HRSD-17 scores). Responders demonstrate a significant negative correlation ($r = -0.56$, $p < 0.0001$) while non-responders show no significant relationship ($r = -0.04$, $p = 0.71$). This relationship indicates that responders with higher inhibitory feedback prior to treatment had lower post-treatment depression severity, suggesting that iTBS may exert its therapeutic effects by enhancing inhibitory mechanisms within local neural circuits. **(C)** E/I balance for responders (green) and non-responders (orange) before (Pre-iTBS) and after (Post-iTBS) treatment, shown as boxplots (median, interquartile range, and whiskers) with individual subject values overlaid. A significant increase in inhibition (reduction in E/I ratio) is observed in responders only following treatment. Note the substantial variability in E/I ratios, particularly at baseline, reflecting individual differences in neurophysiology.

Subgenual-prefrontal interaction is associated with iTBS therapy response

Because the preceding analyses identified relatively global changes, we tested whether pretreatment whole-brain models contained spatial patterns associated with clinical outcome. Mean-centered partial least squares (PLS) analysis within the nested cross-validation framework identified a significant pretreatment latent variable differentiating responders from non-responders (Fig. 4A; $p=0.001$, permutation testing on the training data). Across 100 cross-validation splits, the left sgACC had the strongest discriminative regional loading based exclusively on training-fold decompositions, and the left sgACC and stimulated left DLPFC had loadings with opposite signs (Fig. 4A,B). This relationship is consistent with fMRI findings linking stronger negative DLPFC–sgACC connectivity to better rTMS outcomes (17–19,43). The latent variable is a statistical covariance pattern rather than a distinct biological mechanism; its physiological interpretation derives from the model-derived brain states and recovery of the independently implicated circuit. Responders showed a more negative sgACC–DLPFC loading relationship at the group level, although individual distributions overlapped substantially (Fig. 4B).

Analysis of the pretreatment sgACC time course showed greater model-derived sgACC engagement in responders than non-responders after the single-pulse TMS perturbation (Fig. 4C). This difference was confirmed by AUC analysis, with responders showing greater normalized sgACC engagement than non-responders (Fig. 4D; 35.6 ± 4.2 versus 21.8 ± 3.8, $p<0.001$).

To evaluate out-of-sample discrimination, we examined pretreatment sgACC engagement using stratified 10-fold and leave-one-out cross-validation. Ten-fold cross-validation yielded a mean ROC-AUC of 0.653

± 0.140 across held-out folds (Fig. 4E), while the leave-one-out analysis yielded an AUC of 0.645 ± 0.09 (Fig. 4F). Permutation testing with 5,000 random label assignments indicated that the observed discrimination exceeded chance (Fig. 4G; p=0.0084). These results suggest that pretreatment model-derived sgACC engagement contains information associated with subsequent treatment outcome. However, the discrimination was modest, and the finding should be considered exploratory and hypothesis-generating until independently replicated.

Fig. 4. Neural Signatures Predict Clinical Response to iTBS Treatment for Depression. (A) Treatment-distinguishing pattern — the PLS latent variable, a weighted combination of the SVD-derived brain states shown as loadings over cortical regions — that maximizes the difference between responders and non-responders following iTBS treatment. Lateral and medial views highlight the dlPFC and sgACC regions showing opposite eigenvector loading directions. **(B)** Ratio of sgACC/DLPFC loadings within the brain state maps in A) for responders (green) and non-responders (yellow), showing a more negative sgACC/DLPFC loading relationship on average in responders, with substantial overlap between groups. **(C)** Normalized sgACC activation measured by GMFA at pre-iTBS baseline for responders (green) and non-responders (yellow). Time courses demonstrate higher sgACC engagement patterns for responders. **(D)** AUC analysis of sgACC activation for the entire cohort, demonstrating significantly higher normalized engagement in responders compared to non-responders ($p<0.001$), suggesting pre-treatment sgACC activity may serve as a distinguishing biomarker. **(E)** Stratified 10-fold cross-validated discrimination performance across individual folds, where sgACC engagement served as the predictive feature (mean ROC-AUC = 0.653 ± 0.140). Each bar represents out-of-sample classification performance for one fold. **(F)** ROC curve from leave-one-out cross-validation (AUC = 0.645), corroborating the 10-fold results and demonstrating consistent out-of-sample discrimination. **(G)** Permutation test histogram showing that observed classification performance (red line; AUC = 0.645) significantly exceeds chance level (dashed line; p = 0.0084, 5,000 permutations with random label shuffling).

Greater trajectory deviation and increased stability in neural dynamics of iTBS responders

We next examined TMS-evoked activity as trajectories within the three-dimensional state space of the Jansen–Rit model (Fig. 5A). Before treatment, responders and non-responders exhibited broadly similar trajectories near the stable fixed point. After treatment, responders showed a marked contraction of the trajectory toward the fixed point, whereas non-responders showed less pronounced reorganization.

We quantified these dynamics using two complementary measures. Treatment-related trajectory deviation was calculated as the distance between post-iTBS and pre-iTBS trajectories and therefore indexed the magnitude of change relative to each participant's pretreatment dynamics. Attractor stability was calculated as the distance between the post-iTBS trajectory and the stable fixed point, with smaller distances indicating tighter convergence toward the attractor. Although these measures use different reference points and address different properties of the dynamics, they are derived from the same trajectories and should not be considered statistically independent.

Responders showed significantly greater post-versus-pre trajectory deviation than non-responders (Fig. 5B; $t=3.24$, $p<0.01$; 10,000 permutations), indicating a larger treatment-related reconfiguration of the modeled

dynamics. Responders also remained significantly closer to the stable fixed point after treatment (Fig. 5C; $t=2.18$, $p<0.05$; 10,000 permutations), consistent with greater attractor stability. Together, these findings indicate that treatment response was associated with both a larger reorganization of the modeled state-space trajectory and tighter post-treatment convergence toward the fitted system's stable fixed point.

These measures characterize the geometry of the fitted model and cannot be directly equated with clinical or behavioral stability. Accordingly, they should be interpreted as complementary model-derived properties associated with treatment response rather than independent biological mechanisms. Dynamic visualizations of the pretreatment and post-treatment trajectories are provided in Supplementary Videos V1 and V2.

Fig. 5. iTBS selectively reorganizes attractor dynamics in treatment-responsive individuals. (A) Three-dimensional neural trajectories of the treatment-distinguishing brain state (as identified in Fig. 4 for responders (green) and non-responders (yellow), shown pre-iTBS (left) and post-iTBS (right). Pre-treatment, both groups exhibit similar trajectories, remaining near the stable fixed point (black dot). Post-treatment, responders show a marked trajectory contraction and reduced deviation from the fixed point, suggesting greater stability and reduced sensitivity to external stimuli (e.g., TMS). (B) Point-wise Euclidean distances between post-iTBS and pre-iTBS trajectories. Responders display significantly greater trajectory shifts, indicating a more substantial reconfiguration of the treatment-distinguishing brain state following iTBS. (C) Point-wise Euclidean distance from the stable fixed point in the post-iTBS condition. Responders remain consistently closer to the fixed point, suggesting reduced susceptibility to external perturbation and enhanced attractor stability compared to non-responders. These dynamical changes indicate a treatment-induced reconfiguration toward greater state-space stability in responders. Any link between this model-level stability and clinical or behavioural function is indirect and remains speculative. Note that panels B and C characterize complementary aspects of the same treatment-induced reconfiguration — its magnitude and its endpoint stability — and, being derived from the same trajectories, are not statistically independent.

Journal Pre-proof

DISCUSSION

This study identified three complementary features associated with successful iTBS in TRD: greater low-frequency TMS-evoked power reduction with stronger inhibitory control, a pretreatment DLPFC–sgACC pattern associated with subsequent response, and treatment-related reconfiguration of model-derived neural trajectories. Integrating TMS-EEG with connectome-based whole-brain modeling (37,38) linked electrophysiological measures to fitted circuit parameters and network dynamics, providing a multiscale account of response. However, these findings remain associative and model-derived rather than direct demonstrations of therapeutic mechanisms.

Spectral markers of iTBS efficacy

Responders showed a greater reduction in 3–10 Hz TMS-evoked power following iTBS. This converged with reduced pyramidal-to-excitatory (P→E) drive and strengthened inhibitory-to-pyramidal (I→P) feedback, shifting the model toward greater inhibitory control. Cortical inhibitory deficits in MDD have been demonstrated using TMS-EEG (12); our companion analysis linked iTBS-induced N45 and N100 changes to response (30), and our earlier modeling showed that TEPs emerge from the recurrent E/I loop dynamics captured by these parameters (38). Thus, the fitted parameters provide a circuit-level interpretation of the empirical effect, moving from indirect TEP indices toward an explicit model-based account of altered E/I dynamics.

This interpretation is consistent with evidence that inhibitory microcircuits shape cortical oscillations and responsivity (44,45). TMS-EEG can characterize glutamatergic and GABAergic neurotransmission (46), and effective brain stimulation can suppress pathological low-frequency oscillations by regularizing firing patterns (47). Although not equivalent to the present paradigm, these findings support a broader relationship between inhibition, stimulation, and low-frequency dynamics. Theta-frequency responsiveness of inhibitory interneurons depends partly on membrane properties, including HCN-channel distributions (48,49), while neural-mass models show that extrinsic inputs and synaptic time constants reshape oscillatory regimes (50). Accordingly, reducing P→E connectivity in our simulations increased modeled inhibitory influence and reduced low-frequency power, paralleling the empirical responder effect. This convergence supports a plausible inhibitory account without implying a unique cellular mechanism.

Modeled inhibitory changes associated with clinical improvement

In responders, stronger pretreatment I→P feedback was associated with lower post-treatment clinical scores; I→P subsequently increased in responders but decreased in non-responders, and only responders shifted toward greater inhibition after iTBS. This occurred alongside reduced P→E drive. Together, reduced excitatory amplification and strengthened inhibitory feedback provide a coherent model-based

account of responder physiology, consistent with the goal of using whole-brain models to identify features of stimulation response (24,51,52).

The direction of iTBS-induced plasticity may depend on dose and baseline cortical state. Calcium-dependent models propose that intracellular calcium determines whether stimulation produces potentiation- or depression-like effects (53), and modeling predicts that varying the standard 600-pulse protocol, including 300- and 1200-pulse protocols, can reverse its effect and favor inhibition (54). Prolonged theta-burst stimulation can similarly reverse expected motor-cortical after-effects (55). Participants received 1200 pulses per day, and responders shifted toward inhibition, suggesting that pulse count may contribute to this change. However, baseline state, calcium dynamics, stimulation spacing, and metaplasticity likely also contribute to heterogeneous individual effects.

Recent rodent studies showed that accelerated iTBS engages intratelencephalic prefrontal projection neurons, increasing their activity, spine density, and excitatory currents; chemogenetic silencing abolished the antidepressant-like effect (56,57). This potentiation-like mechanism may appear to contrast with greater modeled inhibitory control in our responders, but the studies differ in protocol and scale. The rodent studies examined accelerated iTBS and projection-defined excitatory populations, whereas our participants received 1200 pulses daily and our three-population model captures net E/I dynamics. Excitatory activation could therefore coexist with greater population-level inhibition through feedback inhibitory recruitment. Moreover, the rodent studies directly measured cellular changes, whereas our parameters were inferred from human TMS-evoked responses. The findings are thus complementary, but our model cannot adjudicate cell-type-specific mechanisms.

Under the GABAergic-deficit hypothesis of depression, supported by reduced GABA and cortical inhibition in MDD, including in the DLPFC (11,12), increased post-treatment inhibitory feedback could reflect partial restoration of deficient control. Reduced prefrontal mGluR5 availability further implicates glutamatergic regulation in disrupted E/I balance (58,59). Enhanced inhibition might improve regulation of rumination or negative cognition, but this remains speculative. Individual differences in anatomy, baseline physiology, and metaplasticity may cause identical protocols to engage different populations or effects. These sources of variability could eventually inform individualized stimulation intensity or pulse number, but this will require subject-specific structural connectivity and prospective validation. Because our models used a normative connectome, the identified physiological features remain candidate markers rather than immediately deployable personalization tools.

Frontolimbic patterns associated with treatment response

Whole-brain modeling relates empirical TMS-EEG responses to distributed patterns of model-derived population activity. Mean-centered PLS identified a pretreatment pattern differentiating responders and

non-responders, with the strongest loadings in the left DLPFC and sgACC and opposite signs across these regions. This statistical covariance pattern is not a biological mechanism, but its expression over physiologically defined model states and recovery of the independently implicated circuit support a circuit-level interpretation.

The sgACC is connected with prefrontal and limbic regions implicated in depression and has been associated with response across antidepressant interventions (60–63). fMRI studies show that stimulating DLPFC sites with stronger negative sgACC connectivity is associated with better outcomes (17–20,43), including substantially greater improvement than stimulation at more distant sites (18). Our opposite-polarity DLPFC–sgACC pattern is therefore consistent with this replicated literature, although it is not equivalent to resting-state functional anticorrelation.

TMS-EEG and resting-state fMRI operate at different temporal and physiological scales but may reflect common anatomical pathways and circuit-excitability properties. Responders also showed greater model-derived sgACC engagement following pretreatment single-pulse TMS, suggesting that DLPFC–sgACC circuit properties may influence susceptibility to iTBS (64,65). However, sgACC activity was inferred through the anatomically constrained model rather than measured directly. Given the substantial group overlap and modest cross-validated discrimination, this finding remains exploratory and hypothesis-generating.

Neural trajectory analysis provided a complementary description of treatment-related changes in model dynamics. Although responders and non-responders showed broadly similar pretreatment trajectories, responders exhibited greater trajectory contraction following iTBS and remained closer to the model's fixed-point attractor (Fig. 5). These findings indicate that treatment response was associated with a reconfiguration toward greater stability within the fitted model's low-dimensional state space.

This dynamical interpretation complements the findings concerning E/I balance and DLPFC–sgACC interactions by describing how treatment-related physiological changes alter the evolution of modeled neural activity over time. However, attractor stability is a property of the fitted model, and its relationship to clinical or behavioral function remains indirect. Greater stability could hypothetically reflect more regulated neural dynamics, but the present data do not establish that relationship. The trajectory changes should therefore be considered a candidate dynamical signature of response rather than a demonstrated therapeutic mechanism or treatment-guidance measure.

Limitations and future directions

Several limitations should be considered. First, the Jansen–Rit neural-mass model necessarily provides a coarse-grained representation of cortical dynamics. Its fitted connectivity parameters represent effective population-level interactions rather than direct measurements of synaptic efficacy, and the model cannot

resolve specific cellular or molecular mechanisms. The present implementation also assumes spatially homogeneous local physiology across cortical regions. Future work could incorporate regional heterogeneity constrained by anatomical, functional, or transcriptional gradients and subject-specific structural connectivity to better capture individual differences in cortical physiology and anatomy.

Second, the present analysis did not include a sham-treated comparator, limiting our ability to distinguish iTBS-specific neurophysiological changes from placebo effects, natural symptom fluctuations, regression to the mean, or other nonspecific treatment effects.

Third, the study lacked an independent external validation cohort. Although nested and out-of-sample cross-validation procedures were used for the sgACC analyses, the broader findings were discovered and evaluated within the same clinical cohort. Independent multisite studies with larger and more diverse cohorts will therefore be important for evaluating their reproducibility and generalizability.

Fourth, sgACC activity was not measured directly but inferred from its interactions with cortical regions through the anatomically constrained whole-brain model. The resulting sgACC signals should therefore be considered exploratory model-derived inferences. Their convergence with independent fMRI evidence concerning DLPFC–sgACC connectivity provides external support but does not constitute direct validation; future studies combining TMS-EEG with concurrent fMRI or intracranial recordings could directly test these inferred dynamics.

Finally, participants received 1200 iTBS pulses per treatment day rather than the standard 600-pulse protocol commonly used in clinical practice, and treatment resistance was defined using an Antidepressant Treatment History Form–Short Form score ≥3 (71). These protocol and clinical-sample characteristics should be considered when generalizing the findings to other iTBS protocols or more severely treatment-resistant populations.

Journal Pre-proof

Journal Pre-proof

ACKNOWLEDGEMENTS AND DISCLOSURES

This work was supported by the CAMH Discovery Fund Talent Competition 2023-24 (D.M.), Krembil Foundation (JG), Canadian Institute of Health Research (JG), Labatt Family Foundation (JG). The CARTBIND study was funded by Brain Canada with the financial assistance of Health Canada, the Temerty Centre for Therapeutic Brain Intervention, Philantropic donation to the NINET lab, Seedlings Foundation, the Krembil Family Foundation, the Arrell Family Foundation, and the Toronto General and Western Hospital Foundation.

All authors report no biomedical financial interests or potential conflicts of interest.

A previous version of this manuscript was posted as a preprint on bioRxiv (https://doi.org/10.1101/2025.04.23.648963).

Supplement Description (3 files):

Supplement Methods, Results, Figures S1-S4, Table S1, Video Legends

Video S1

Video S2

Journal Pre-proof

REFERENCES

1. Kessler RC (2012): The costs of depression. *Psychiatr Clin North Am* 35: 1–14.
2. Rush AJ, Trivedi MH, Wisniewski SR, Nierenberg AA, Stewart JW, Warden D, *et al.* (2006): Acute and longer-term outcomes in depressed outpatients requiring one or several treatment steps: a STAR*D report. *Am J Psychiatry* 163: 1905–1917.
3. Blumberger DM, Vila-Rodriguez F, Thorpe KE, Feffer K, Noda Y, Giacobbe P, *et al.* (2018): Effectiveness of theta burst versus high-frequency repetitive transcranial magnetic stimulation in patients with depression (THREE-D): a randomised non-inferiority trial. *Lancet Lond Engl* 391: 1683–1692.
4. Voineskos D, Daskalakis ZJ, Blumberger DM (2020): Management of Treatment-Resistant Depression: Challenges and Strategies. *Neuropsychiatr Dis Treat* 16: 221–234.
5. Sehatzadeh S, Daskalakis ZJ, Yap B, Tu H-A, Palimaka S, Bowen JM, O'Reilly DJ (2019): Unilateral and bilateral repetitive transcranial magnetic stimulation for treatment-resistant depression: a meta-analysis of randomized controlled trials over 2 decades. *J Psychiatry Neurosci JPN* 44: 151–163.
6. Kaster TS, Fitzgerald PB, Downar J, Vila-Rodriguez F, Daskalakis ZJ, Blumberger DM (2020): Considerable evidence supports rTMS for treatment-resistant depression. *J Affect Disord* 263: 549–551.
7. Berlim MT, van den Eynde F, Tovar-Perdomo S, Daskalakis ZJ (2014): Response, remission and drop-out rates following high-frequency repetitive transcranial magnetic stimulation (rTMS) for treating major depression: a systematic review and meta-analysis of randomized, double-blind and sham-controlled trials. *Psychol Med* 44: 225–239.
8. Fitzgerald PB, Hoy KE, Anderson RJ, Daskalakis ZJ (2016): A study of the pattern of response to rTMS treatment in depression. *Depress Anxiety* 33: 746–753.
9. Rogasch NC, Thomson RH, Farzan F, Fitzgibbon BM, Bailey NW, Hernandez-Pavon JC, *et al.* (2014): Removing artefacts from TMS-EEG recordings using independent component analysis: importance for assessing prefrontal and motor cortex network properties. *NeuroImage* 101: 425–439.
10. Bonato C, Miniussi C, Rossini PM (2006): Transcranial magnetic stimulation and cortical evoked potentials: a TMS/EEG co-registration study. *Clin Neurophysiol Off J Int Fed Clin Neurophysiol* 117: 1699–1707.
11. Hu Y-T, Tan Z-L, Hirjak D, Northoff G (2023): Brain-wide changes in excitation-inhibition balance of major depressive disorder: a systematic review of topographic patterns of GABA- and glutamatergic alterations. *Mol Psychiatry* 28: 3257–3266.
12. Voineskos D, Blumberger DM, Zomorrodi R, Rogasch NC, Farzan F, Foussias G, *et al.* (2019): Altered Transcranial Magnetic Stimulation-Electroencephalographic Markers of Inhibition and Excitation in the Dorsolateral Prefrontal Cortex in Major Depressive Disorder. *Biol Psychiatry* 85: 477–486.
13. Mullins PG, McGonigle DJ, O'Gorman RL, Puts NAJ, Vidyasagar R, Evans CJ, *et al.* (2014): Current practice in the use of MEGA-PRESS spectroscopy for the detection of GABA. *NeuroImage* 86: 43–52.
14. Duman RS, Sanacora G, Krystal JH (2019): Altered Connectivity in Depression: GABA and Glutamate Neurotransmitter Deficits and Reversal by Novel Treatments. *Neuron* 102: 75–90.
15. Godfrey KEM, Gardner AC, Kwon S, Chea W, Muthukumaraswamy SD (2018): Differences in excitatory and inhibitory neurotransmitter levels between depressed patients and healthy controls: A systematic review and meta-analysis. *J Psychiatr Res* 105: 33–44.
16. Dhami P, Moreno S, Croarkin PE, Blumberger DM, Daskalakis ZJ, Farzan F (2023): Baseline markers of cortical excitation and inhibition predict response to theta burst stimulation treatment for youth depression. *Sci Rep* 13: 19115.
17. Weigand A, Horn A, Caballero R, Cooke D, Stern AP, Taylor SF, *et al.* (2018): Prospective Validation That Subgenual Connectivity Predicts Antidepressant Efficacy of Transcranial Magnetic Stimulation Sites. *Biol Psychiatry* 84: 28–37.
18. Cash RFH, Weigand A, Zalesky A, Siddiqi SH, Downar J, Fitzgerald PB, Fox MD (2021): Using Brain Imaging to Improve Spatial Targeting of Transcranial Magnetic Stimulation for Depression. *Biol Psychiatry* 90: 689–700.
19. Fox MD, Buckner RL, White MP, Greicius MD, Pascual-Leone A (2012): Efficacy of Transcranial Magnetic Stimulation Targets for Depression Is Related to Intrinsic Functional Connectivity with the Subgenual Cingulate. *Biol Psychiatry* 72: 595–603.
20. Salomons TV, Dunlop K, Kennedy SH, Flint A, Geraci J, Giacobbe P, Downar J (2014): Resting-State Cortico-Thalamic-Striatal Connectivity Predicts Response to Dorsomedial Prefrontal rTMS in Major Depressive Disorder. *Neuropsychopharmacology* 39: 488–498.

Journal Pre-proof

21. Levy LM, Degnan AJ (2013): GABA-Based Evaluation of Neurologic Conditions: MR Spectroscopy. *AJNR Am J Neuroradiol* 34: 259–265.
22. Steel A, Mikkelsen M, Edden RAE, Robertson CE (2020): Regional balance between glutamate+glutamine and GABA+ in the resting human brain. *NeuroImage* 220: 117112.
23. Pathak A, Roy D, Banerjee A (2022): Whole-Brain Network Models: From Physics to Bedside. *Front Comput Neurosci* 16: 866517.
24. Lang S, Momi D, Vetkas A, Santyr B, Yang AZ, Kalia SK, *et al.* (2024): Computational modeling of whole-brain dynamics: a review of neurosurgical applications. *J Neurosurg* 140: 218–230.
25. Luppi AI, Mediano PAM, Rosas FE, Allanson J, Pickard JD, Carhart-Harris RL, *et al.* (2024): A Synergistic Workspace for Human Consciousness Revealed by Integrated Information Decomposition. *eLife* 12. https://doi.org/10.7554/eLife.88173.3
26. Hofsähs T, Pille M, Kern L, Negi A, Meier JM, Ritter P (2024, November 25): The Virtual Brain links transcranial magnetic stimulation evoked potentials and inhibitory neurotransmitter changes in major depressive disorder. bioRxiv, p 2024.11.25.622620.
27. Meier JM, Perdikis D, Blickensdörfer A, Stefanovski L, Liu Q, Maith O, *et al.* (2022): Virtual deep brain stimulation: Multiscale co-simulation of a spiking basal ganglia model and a whole-brain mean-field model with The Virtual Brain. *Exp Neurol* 354: 114111.
28. Patow G, Stefanovski L, Ritter P, Deco G, Kobeleva X, Alzheimer's Disease Neuroimaging Initiative (2023): Whole-brain modeling of the differential influences of amyloid-beta and tau in Alzheimer's disease. *Alzheimers Res Ther* 15: 210.
29. Wang HE, Woodman M, Triebkorn P, Lemarechal J-D, Jha J, Dollomaja B, *et al.* (2023): Delineating epileptogenic networks using brain imaging data and personalized modeling in drug-resistant epilepsy. *Sci Transl Med* 15: eabp8982.
30. Strafella R, Momi D, Zomorrodi R, Lissemore J, Noda Y, Chen R, *et al.* (2023): Identifying Neurophysiological Markers of Intermittent Theta Burst Stimulation in Treatment-Resistant Depression Using Transcranial Magnetic Stimulation–Electroencephalography. *Biol Psychiatry* 94: 454–465.
31. Van Essen DC, Ugurbil K, Auerbach E, Barch D, Behrens TEJ, Bucholz R, *et al.* (2012): The Human Connectome Project: a data acquisition perspective. *NeuroImage* 62: 2222–2231.
32. Jansen BH, Rit VG (1995): Electroencephalogram and visual evoked potential generation in a mathematical model of coupled cortical columns. *Biol Cybern* 73: 357–366.
33. Schaefer A, Kong R, Gordon EM, Laumann TO, Zuo X-N, Holmes AJ, *et al.* (2018): Local-Global Parcellation of the Human Cerebral Cortex from Intrinsic Functional Connectivity MRI. *Cereb Cortex N Y N 1991* 28: 3095–3114.
34. Rall LB (Ed.) (1981): Examples of software for automatic differentiation and generation of Taylor coefficients. *Automatic Differentiation: Techniques and Applications*. Berlin, Heidelberg: Springer, pp 54–90.
35. Kingma DP, Ba J (2017, January 30): Adam: A Method for Stochastic Optimization [no. arXiv:1412.6980]. arXiv. https://doi.org/10.48550/arXiv.1412.6980
36. Blumberger DM, Vila-Rodriguez F, Wang W, Knyahnytska Y, Butterfield M, Noda Y, *et al.* (2021): A randomized sham controlled comparison of once vs twice-daily intermittent theta burst stimulation in depression: A Canadian rTMS treatment and biomarker network in depression (CARTBIND) study. *Brain Stimulat* 14: 1447–1455.
37. Momi D, Wang Z, Parmigiani S, Mikulan E, Bastiaens SP, Oveisi MP, *et al.* (2025): Stimulation mapping and whole-brain modeling reveal gradients of excitability and recurrence in cortical networks. *Nat Commun* 16: 3222.
38. Momi D, Wang Z, Griffiths JD (2023): TMS-evoked responses are driven by recurrent large-scale network dynamics ((A. Fornito, M. J. Frank, J. Meier, & A. Pigorini, editors)). *eLife* 12: e83232.
39. Mišić B, Betzel RF, de Reus MA, van den Heuvel MP, Berman MG, McIntosh AR, Sporns O (2016): Network-Level Structure-Function Relationships in Human Neocortex. *Cereb Cortex N Y NY* 26: 3285–3296.
40. McIntosh AR, Bookstein FL, Haxby JV, Grady CL (1996): Spatial Pattern Analysis of Functional Brain Images Using Partial Least Squares. *NeuroImage* 3: 143–157.
41. Hamilton M (1960): A rating scale for depression. *J Neurol Neurosurg Psychiatry* 23: 56–62.
42. Lehmann D, Skrandies W (1980): Reference-free identification of components of checkerboard-evoked multichannel potential fields. *Electroencephalogr Clin Neurophysiol* 48: 609–621.
43. Hearne LJ, Webb L, Cash R, Robinson C, Mosley PE, Ng J, *et al.* (2025): Clinical and Neurophysiological Effects of Robotically-Delivered fMRI-Guided Personalized Transcranial Magnetic Stimulation Therapy for Depression. *Psychother Psychosom*. https://doi.org/10.1159/000545692

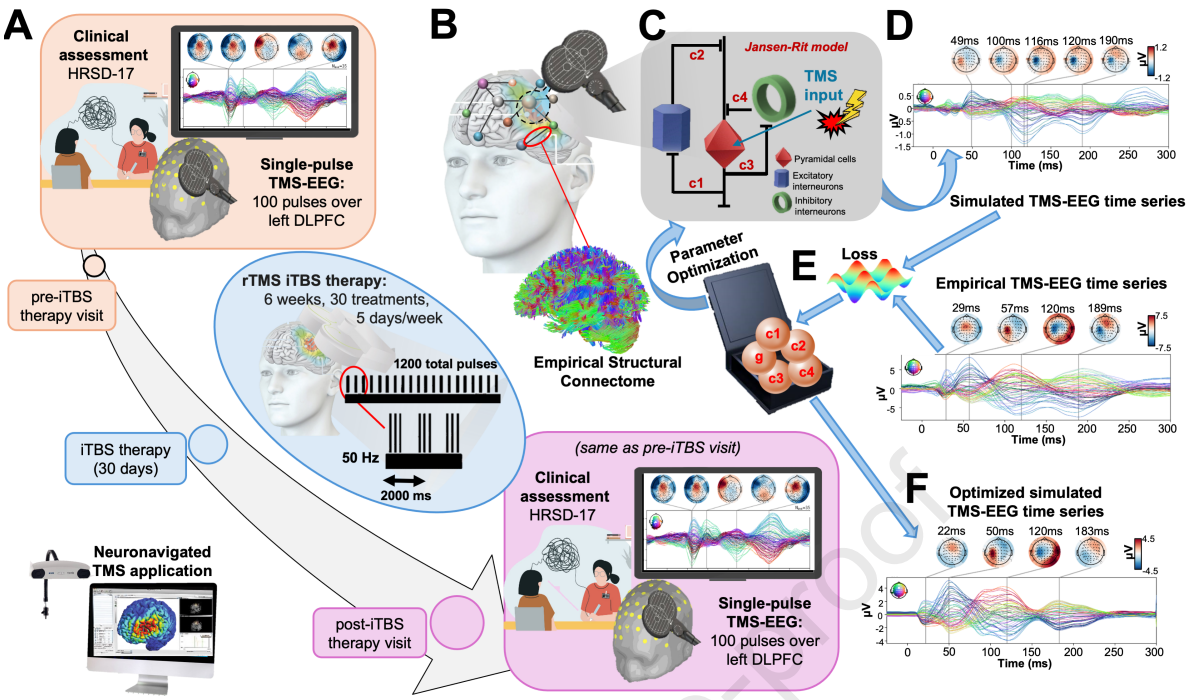
Journal Pre-proof

44. Carlén M, Meletis K, Siegle JH, Cardin JA, Futai K, Vierling-Claassen D, *et al.* (2012): A critical role for NMDA receptors in parvalbumin interneurons for gamma rhythm induction and behavior. *Mol Psychiatry* 17: 537–548.
45. Letzkus JJ, Wolff SBE, Meyer EMM, Tovote P, Courtin J, Herry C, Lüthi A (2011): A disinhibitory microcircuit for associative fear learning in the auditory cortex. *Nature* 480: 331–335.
46. Cash RFH, Noda Y, Zomorrodi R, Radhu N, Farzan F, Rajji TK, *et al.* (2017): Characterization of Glutamatergic and GABAA-Mediated Neurotransmission in Motor and Dorsolateral Prefrontal Cortex Using Paired-Pulse TMS–EEG. *Neuropsychopharmacology* 42: 502–511.
47. McConnell GC, So RQ, Hilliard JD, Lopomo P, Grill WM (2012): Effective Deep Brain Stimulation Suppresses Low-Frequency Network Oscillations in the Basal Ganglia by Regularizing Neural Firing Patterns. *J Neurosci* 32: 15657–15668.
48. Freund TF, Buzsáki G (1996): Interneurons of the hippocampus. *Hippocampus* 6: 347–470.
49. Sekulić V, Skinner FK (2017): Computational models of O-LM cells are recruited by low or high theta frequency inputs depending on h-channel distributions ((J. Huguenard, editor)). *eLife* 6: e22962.
50. Spiegler A, Kiebel SJ, Atay FM, Knösche TR (2010): Bifurcation analysis of neural mass models: Impact of extrinsic inputs and dendritic time constants. *NeuroImage* 52: 1041–1058.
51. Jung K, Florin E, Patil KR, Caspers J, Rubbert C, Eickhoff SB, Popovych OV (2023): Whole-brain dynamical modelling for classification of Parkinson's disease. *Brain Commun* 5: fcac331.
52. Kurtin DL, Giunchiglia V, Vohryzek J, Cabral J, Skeldon AC, Violante IR (2023): Moving from phenomenological to predictive modelling: Progress and pitfalls of modelling brain stimulation in-silico. *NeuroImage* 272: 120042.
53. Wilson MT, Fulcher BD, Fung PK, Robinson PA, Fornito A, Rogasch NC (2018): Biophysical modeling of neural plasticity induced by transcranial magnetic stimulation. *Clin Neurophysiol* 129: 1230–1241.
54. Fung PK, Robinson PA (2014): Neural field theory of synaptic metaplasticity with applications to theta burst stimulation. *J Theor Biol* 340: 164–176.
55. Gamboa OL, Antal A, Moliadze V, Paulus W (2010): Simply longer is not better: reversal of theta burst after-effect with prolonged stimulation. *Exp Brain Res* 204: 181–187.
56. Gongwer MW, Qi A, Enos AS, Mora SAR, Solakoğlu ST, Ahmed RN, *et al.* (2026): A cell type-specific mechanism driving the rapid antidepressant effects of transcranial magnetic stimulation. *Cell* 189: 3052-3070.e13.
57. Johnson SB, Rocks D, Chalençon L, Johnson K, Hassan U, Arefin A, *et al.* (2026): Fronto-insular circuit mechanisms of accelerated intermittent theta burst stimulation. *Cell* 189: 3071-3090.e27.
58. Pin JP, Duvoisin R (1995): The metabotropic glutamate receptors: structure and functions. *Neuropharmacology* 34: 1–26.
59. Deschwanden A, Karolewicz B, Feyissa AM, Treyer V, Ametamey SM, Johayem A, *et al.* (2011): Reduced metabotropic glutamate receptor 5 density in major depression determined by [(11)C]ABP688 PET and postmortem study. *Am J Psychiatry* 168: 727–734.
60. Riva-Posse P, Choi KS, Holtzheimer PE, Crowell AL, Garlow SJ, Rajendra JK, *et al.* (2018): A connectomic approach for subcallosal cingulate deep brain stimulation surgery: prospective targeting in treatment-resistant depression. *Mol Psychiatry* 23: 843–849.
61. Drevets WC, Savitz J, Trimble M (2008): The subgenual anterior cingulate cortex in mood disorders. *CNS Spectr* 13: 663–681.
62. Siegle GJ, Thompson WK, Collier A, Berman SR, Feldmiller J, Thase ME, Friedman ES (2012): Toward clinically useful neuroimaging in depression treatment: prognostic utility of subgenual cingulate activity for determining depression outcome in cognitive therapy across studies, scanners, and patient characteristics. *Arch Gen Psychiatry* 69: 913–924.
63. Hamani C, Mayberg H, Stone S, Laxton A, Haber S, Lozano AM (2011): The subcallosal cingulate gyrus in the context of major depression. *Biol Psychiatry* 69: 301–308.
64. Cole EJ, Stimpson KH, Bentzley BS, Gulser M, Cherian K, Tischler C, *et al.* (2020): Stanford Accelerated Intelligent Neuromodulation Therapy for Treatment-Resistant Depression. *Am J Psychiatry* 177: 716–726.
65. Padmanabhan JL, Cooke D, Joutsa J, Siddiqi SH, Ferguson M, Darby RR, *et al.* (2019): A Human Depression Circuit Derived From Focal Brain Lesions. *Biol Psychiatry* 86: 749–758.
66. Deco G, Kringelbach ML, Arnatkeviciute A, Oldham S, Sabaroedin K, Rogasch NC, *et al.* (2021): Dynamical consequences of regional heterogeneity in the brain's transcriptional landscape. *Sci Adv* 7: eabf4752.

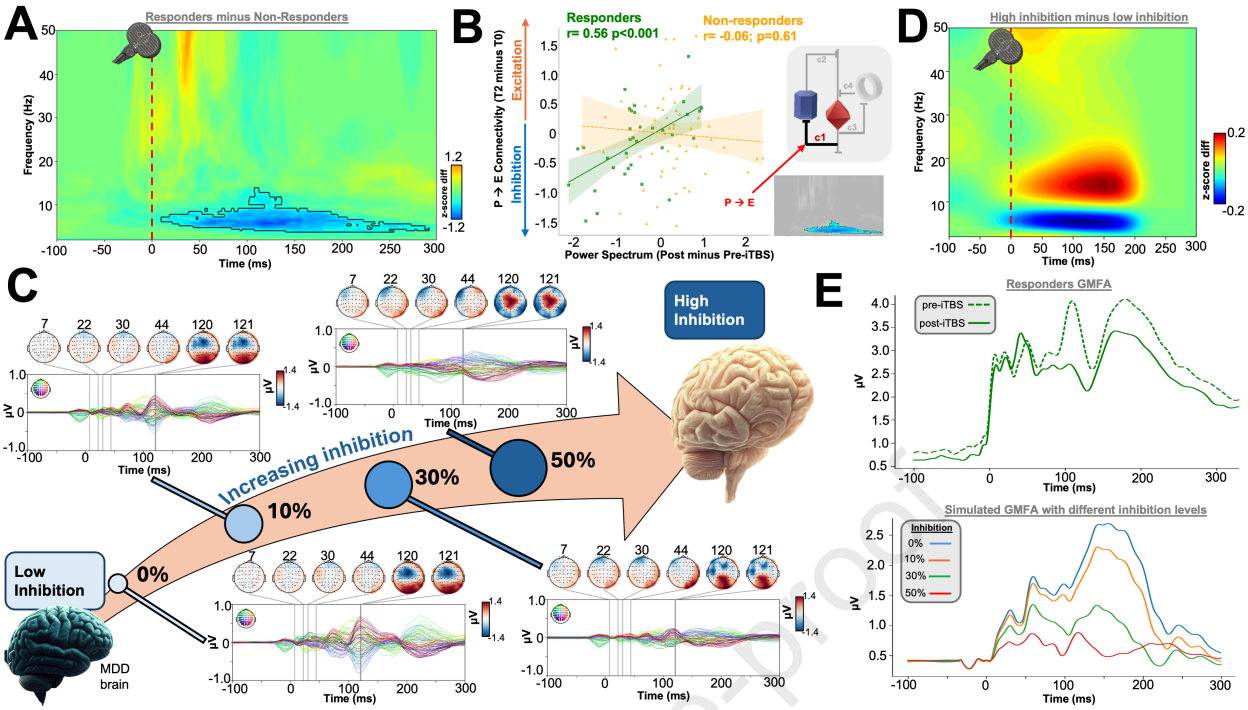
Journal Pre-proof

67. Idesis S, Allegra M, Vohryzek J, Perl YS, Metcalf NV, Griffis JC, *et al.* (2024): Generative whole-brain dynamics models from healthy subjects predict functional alterations in stroke at the level of individual patients. *Brain Commun* 6: fcae237.
68. Deco G, Kringelbach ML (2014): Great Expectations: Using Whole-Brain Computational Connectomics for Understanding Neuropsychiatric Disorders. *Neuron* 84: 892–905.
69. Shine JM (2021): The thalamus integrates the macrosystems of the brain to facilitate complex, adaptive brain network dynamics. *Prog Neurobiol* 199: 101951.
70. Müller EJ, Munn BR, Shine JM (2020): Diffuse neural coupling mediates complex network dynamics through the formation of quasi-critical brain states. *Nat Commun* 11: 6337.
71. Sackeim HA, Aaronson ST, Bunker MT, Conway CR, Demitrack MA, George MS, *et al.* (2019): The assessment of resistance to antidepressant treatment: Rationale for the Antidepressant Treatment History Form: Short Form (ATHF-SF). *J Psychiatr Res* 113: 125–136.

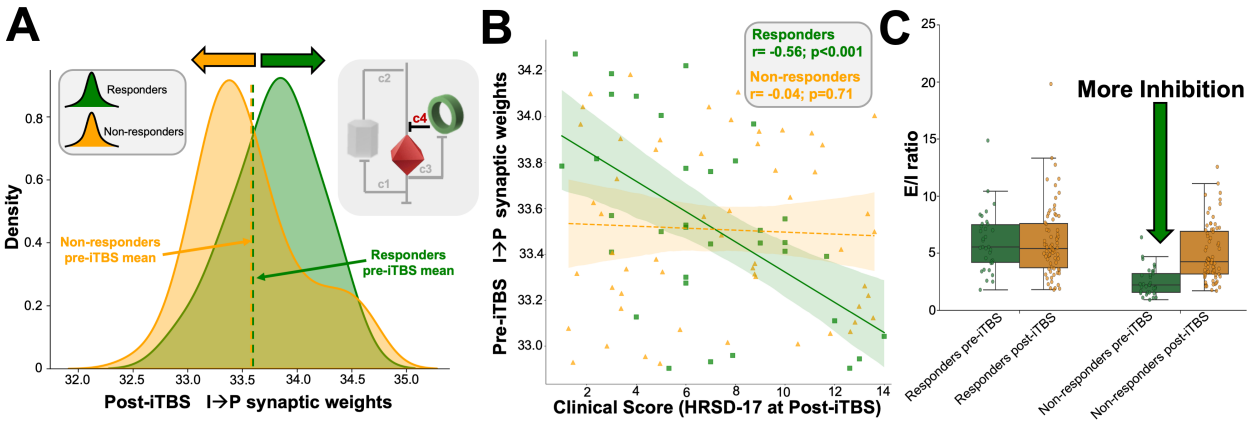
Journal Pre-proof



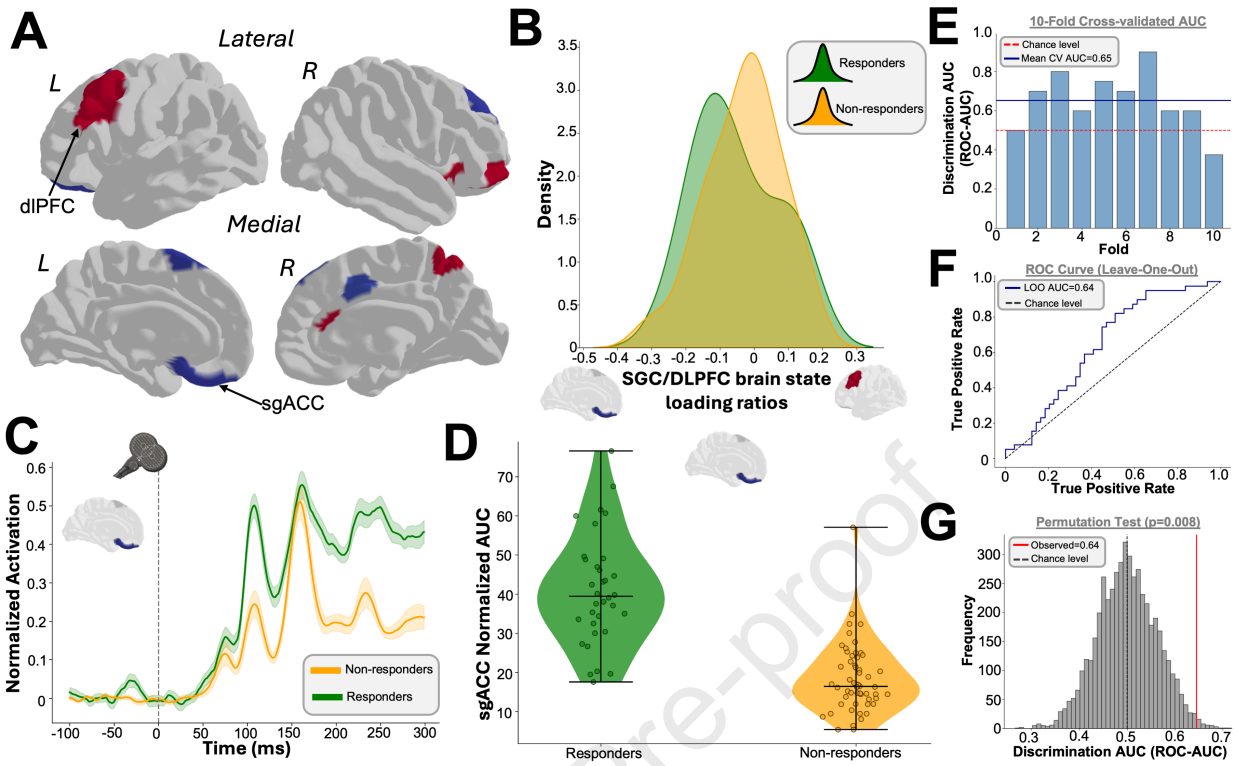
Journal Pre-proof



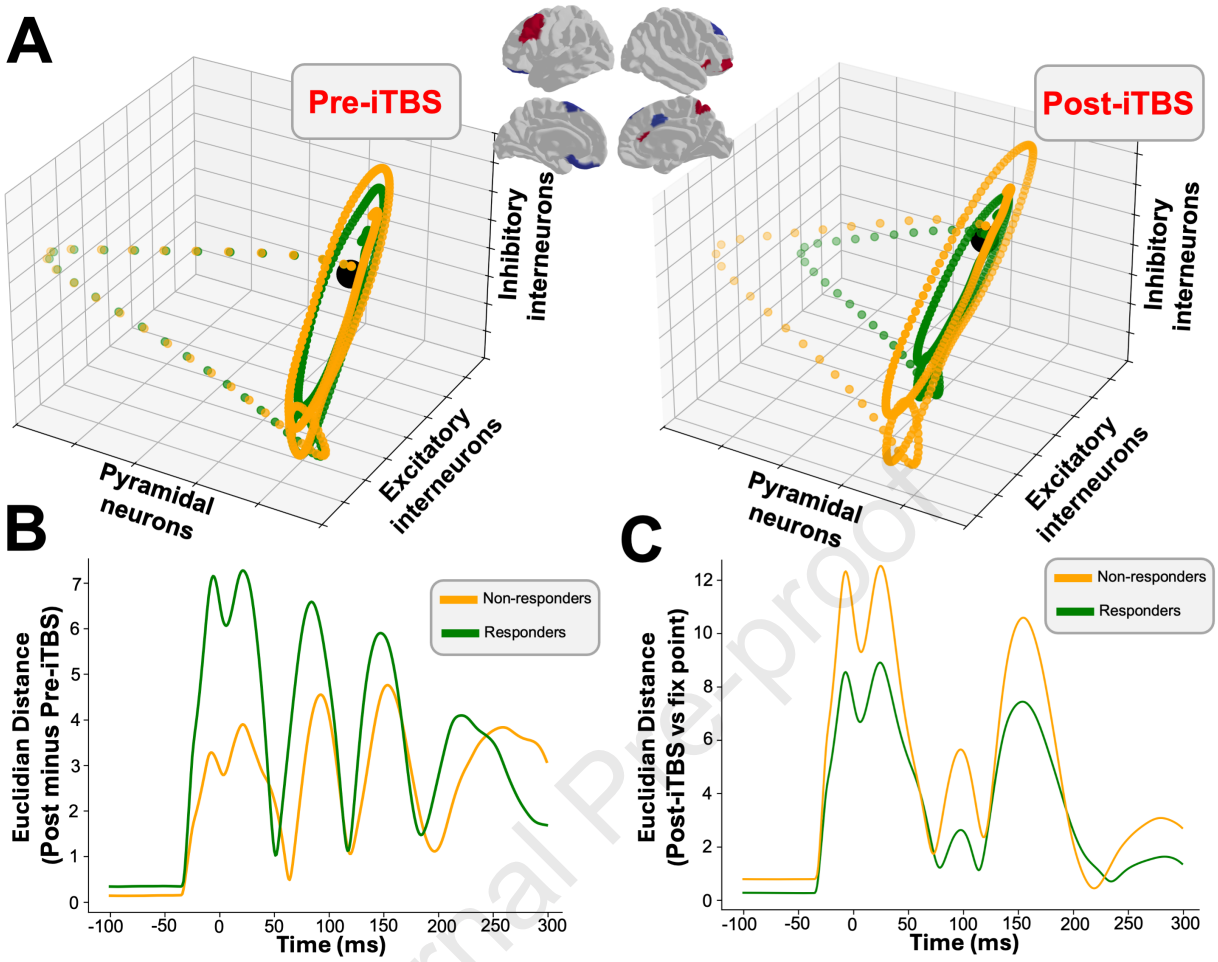
Journal Pre-proof



Journal Pre-proof



Journal Pre-proof



Journal Pre-proof